Main Results of the PICARD mission

M. Meftah[a,*], T. Corbard[b], A. Hauchecorne[a], A. Irbah[a], P. Boumier[c], A. Chevalier[d], W. Schmutz[e], R. Ikhlef[b,i], F. Morand[b], C. Renaud[b], J.-F. Hochedez[a,h], G. Cessateur[e,j], S. Turck-Chièze[f], D. Salabert[b,f], M. Rouzé[g], M. van Ruymbeke[h], P. Zhu[h], S. Kholikov[k], S. Koller[e], C. Conscience[d], S. Dewitte[d], L. Damé[a], and D. Djafer[l]

[a] Université Paris Saclay, Université Paris VI - Pierre et Marie Curie, CNRS/INSU, LATMOS-IPSL, 11 Boulevard d'Alembert, 78280 Guyancourt, France
[b] Laboratoire Lagrange, Université de Nice Sophia-Antipolis, CNRS, Observatoire de la Côte d'Azur, Boulevard de l'Observatoire, 06304 Nice, France
[c] IAS, CNRS, Université Paris XI, 91471 Orsay, France
[d] RMIB, 3 Avenue Circulaire, 1180 Bruxelles (Uccle), Belgique
[e] PMOD/WRC, Dorfstrasse 33, 7260 Davos Dorf, Switzerland
[f] IRFU, CEA-Saclay, 91191 Gif-sur-Yvette Cedex, France
[g] CNES, Rue Edouard Belin, 31000 Toulouse, France
[h] ROB, 3 Avenue Circulaire, 1180 Bruxelles (Uccle), Belgique
[i] CRAAG, Observatoire d'Alger, Alger, Algérie
[j] BIRA-IASB, Ringlaan 3, 1180 Brussels, Belgium
[k] National Solar Observatory, Tucson, Arizona, United States of America
[l] Unité de Recherche Appliquée en Energies Renouvelables, URAER, Centre de Développement des Energies Renouvelables, CDER, 47133, Ghardaïa, Algérie

ABSTRACT

PICARD is a mission devoted to solar variability observations through imagery and radiometric measurements. The main goal is to provide data for scientific investigation first in the area of solar physics, and second in the assessment of the influence of the solar variability on the Earth climate variability. PICARD contains a double program with in-space and on-ground measurements. The PICARD spacecraft was launched on June 15, 2010, commissioned in-flight in October of the same year and was retired in April 2014. The PICARD ground-based observatory is operational since May 2011. We shall give a short overview of the PICARD instrumentation. New estimates of the absolute values of the total solar irradiance, of the solar spectral irradiance at typical wavelengths, and of the solar oblateness will be given. We will also report about helioseismic studies. Finally, we will present our current results about solar radius variations after six years of solar observation.

Keywords: Sun, PICARD, Spacecraft, Ground-based observatory, TSI, SSI, Solar oblateness, Helioseismology, Solar radius, Image-processing methods.

1. INTRODUCTION

The PICARD mission expands observations of the global parameters of the Sun with the hope to link the variability of its total and spectral irradiance to its geometric shape (chiefly its diameter and oblateness). These measurements represent key inputs to validate solar models and to understand the origin of the solar activity. To achieve the PICARD scientific objectives, the following measurement were carried out:

- Total Solar Irradiance (TSI) by two independent space-based radiometers,

* Corresponding author
E-mail address: Mustapha.Meftah@latmos.ipsl.fr

Space Telescopes and Instrumentation 2016: Optical, Infrared, and Millimeter Wave, edited by Howard A. MacEwen, Giovanni G. Fazio, Makenzie Lystrup, Proc. of SPIE Vol. 9904, 99040Z · © 2016 SPIE · CCC code: 0277-786X/16/$18 · doi: 10.1117/12.2232027

- Solar Spectral Irradiance (SSI) at several wavelengths using a space-based photometer, a space-based solar sensor, and a space-based imaging telescope,
- Solar oblateness by a space-based imaging telescope,
- Solar oscillations (helioseismology) by a space-based imaging telescope,
- Solar diameter using a space-based imaging telescope and a ground-based imaging telescope with its associated instrumentation.

Figure 1: (left) Artist's view of the PICARD spacecraft. Credits: CNES - D. Ducros.
(right) PICARD spacecraft with its scientific payload during integration phase in 2009.

Figure 2: PICARD SOL with its two main scientific instruments (SODISM II and MISOLFA) in 2016.

The present document displays the status of the PICARD mission, which contains a double program with in-space (PICARD spacecraft) and on-ground measurements (PICARD SOL).

1. The space measurements were carried out by the PICARD spacecraft (Figure 1) with the following scientific instruments:
   - PREcision MOnitoring Sensor (PREMOS[1]) is a set of three Sun-photometers (observations at 210, 215, 266, 535, 607, and 782 nm) and a PMO6 radiometer type (absolute cavity pyrheliometer) as used on Solar and Heliospheric Observatory (SoHO) to measure the total solar irradiance. PREMOS instrument is under the responsibility of the Physikalisch-Meteorologisches Observatorium Davos (PMOD, Switzerland).

- SOlar VAriability PICARD (SOVAP[2,3]) instrument provided by the Royal Meteorological Institute of Belgium (RMIB, Belgium) measures the total solar irradiance. This instrument is a radiometer of DIfferential Absolute RADiometer (DIARAD) type used in previous space missions (SOLar CONstant instrument (SOLCON) on Spacelab and onboard the space shuttle, the Solar Variations (SOVA 1) experiment onboard European Retrievable Carrier (EURECA), DIARAD onboard SoHO, the Sun Monitoring on the External Payload Facility of Columbus-SOlar Variable and Irradiance Monitor (Solar-SOVIM)). There is also a bolometer provided by the Royal Observatory of Belgium (ROB).
- SOlar Diameter Imager and Surface Mapper (SODISM[4]) developed by the Centre National de la Recherche Scientifique (CNRS, France) is an imaging Ritchey-Chrétien telescope for measuring the solar diameter and the solar oblateness (535.7, 607.1, and 782.2 nm in the photospheric continuum). It performs also helioseismic observations (535.7 nm) to probe the solar interior. Images in the Ca II line (393.37 nm) are used to detect active regions near the solar limb, which may impact the diameter measurements. These observations (393.37, 535.7, 607.1, and 782.2 nm) could be used to measure the solar spectral irradiance and the solar differential rotation as well as for space weather, together with images in the 215 nm wavelength.

2. The ground-based measurements were carried out by PICARD SOL[5] at the Observatoire de la Côte d'Azur (OCA, France) in the Calern site as shown in Figure 2. PICARD SOL aim is to perpetuate valuable historical series of the solar radius and to better understand the effects of the atmosphere on solar radius measurements. The main instruments of PICARD SOL are described below:
   - SODISM II[5] (a copy of the SODISM space instrument) is a multi-wavelength full disc solar imager (observations at 393.37, 535.7, 607.1, 782.2, and 1025.0 nm) specially designed for metrological solar radius measurements. SODISM II instrument is under the responsibility of "Laboratoire Atmosphères, Milieux, Observations Spatiales" (LATMOS, France) from CNRS.
   - "Moniteur d'Images Solaires Franco-Algérien" (MISOLFA[6]) is a high-cadence solar limb imager allowing us to measure the spatio-temporal parameters of the local turbulence. Ground-based solar observations are strongly affected by optical turbulence. MISOLFA turbulence monitor is under the responsibility of OCA.

In this article, we report on PICARD main results, which were obtained during Solar Cycle 24. Some studies have been published and others are still under investigation. Studies under development will be more developed.

2. TOTAL SOLAR IRRADIANCE (TSI)

The TSI value is crucial for solar physics and for the Sun-Earth connection. The PICARD space-based TSI radiometers (PREMOS and SOVAP) have helped to resolve the conflict about the absolute TSI value as measured by the Total Irradiance Monitor (TIM[7]) instrument onboard SOlar Radiation and Climate Experiment (SORCE) and Variability of IRradiance and Gravity Oscillations (VIRGO[8]) experiment onboard SoHO. As a reminder, the consensus absolute value of the TSI was close to $1365.4 \pm 1.3\,\mathrm{Wm}^{-2}$ prior to the SORCE launch. SORCE/TIM measured deviating values[7] of $1360.8 \pm 0.5\,\mathrm{Wm}^{-2}$ during the 2008 solar minimum period.

With a first light measurement around $1360.9 \pm 0.4\,\mathrm{Wm}^{-2}$, the PREMOS instrument confirmed the lower value of the TSI as measured by the SORCE/TIM instrument. Both instruments are in excellent agreement within the combined uncertainties of the two instruments.[9] It appears that stray light contribution has been significantly underestimated within the SoHO/VIRGO instrument.[10]

SOVAP absolute TSI is equal to $1361.8 \pm 2.4\,\mathrm{Wm}^{-2}$ for a quiet Sun (solar minimum). To determine the TSI from SOVAP, a new instrument equation was established.[3] A parameter was integrated from a theoretical analysis that highlighted the thermo-electrical non-equivalence of the DIARAD radiometric cavity. From this approach, the TSI values are lower than those previously provided with the same type of instruments.

TIM, PREMOS, and SOVAP show lower TSI than the canonical value of $1365.4 \pm 1.3\,\mathrm{Wm}^{-2}$ used a decade ago.

3. SOLAR SPECTRAL IRRADIANCE (SSI)

3.1 SSI from PREMOS Measurements

The PREMOS instrument measured the solar spectral irradiance. Several measurements were carried out in the UV spectral band (at 210, 215, and 266 nm), in the visible band (at 535 and 607 nm), and in the near-infrared band (at 782 nm). Using a redundancy strategy as well as some proxy models, the UV channels have been successfully corrected,[11] and are in a very good agreement with other observational data sets such as SOLar STelar Irradiance Comparison Experiment (SOLSTICE) onboard SORCE as displayed in Figure 3. Regarding the PREMOS UV channels, there is an excellent correlation over the lifetime of the PICARD space mission. The ratio between SORCE/SOLSTICE and PREMOS observations is always less than 1%. Regarding the SSI measurements in the visible and near-infrared, a comparison of short-term variations (*i.e.* 27-day modulation) shows a rather good correlation by taking into consideration the intrinsic noise within both Spectral Irradiance Monitor (SIM[12]) and PREMOS observations.[11] A detailed analysis is required in order to compare all PICARD SSI results (PREMOS, SES, and future SODISM SSI) with the SSI as seen by the SOLar SPECtrum (SOLSPEC) instrument (SSI measurements from 165 to 3088 nm) of the solar monitoring observatory payload (SOLAR) onboard the International Space Station (ISS).

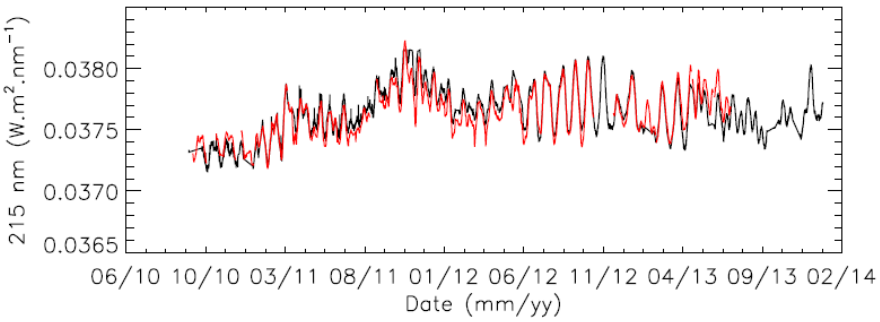

Figure 3: Level 3 PREMOS data for the solar irradiance at 215 nm (in red) compared to SORCE/SOLSTICE observations convolved with the PREMOS filter bandpass (in black).

3.2 SSI from the SES Sensor Measurements

A Sun Ecartometry Sensor (SES) was developed to provide the stringent pointing requirements of the PICARD spacecraft. From the SES data, we obtained a new time series of the solar spectral irradiance at 782 nm[13] from 2010 to 2014 (Figure 4). A comparison between PREMOS and the SES SSI at 782 nm is under evaluation.

3.3 SSI from SODISM Images (work in progress)

There is a great interest to provide SSI evolution from SODISM images (links with PREMOS, the SES, and the solar radius). SODISM has probably a sufficient quality to feed SSI models despite a significant image blurring[4] and a point spread function (psf) change. There is still a considerable optical modeling effort. The correspondence of SODISM and PREMOS spectral channels offers a supplementary leverage that ought to be exploited in the future (with all SODISM corrections).

List of instrumental effects in the SODISM space-based telescope are:

- Additive (offset, dark signal, cosmic ray hits, ghost images, *etc.*),
- Multiplicative (optical flat field, charge-coupled device (CCD) flat field, non linearity of the detection, *etc.*),
- Convolutive (psf (scattered light, kinematic blur, optical aberrations), persistence/hysteresis, CCD charge transfer efficiency),
- and other effects (distortion (anamorphosis), *etc.*).

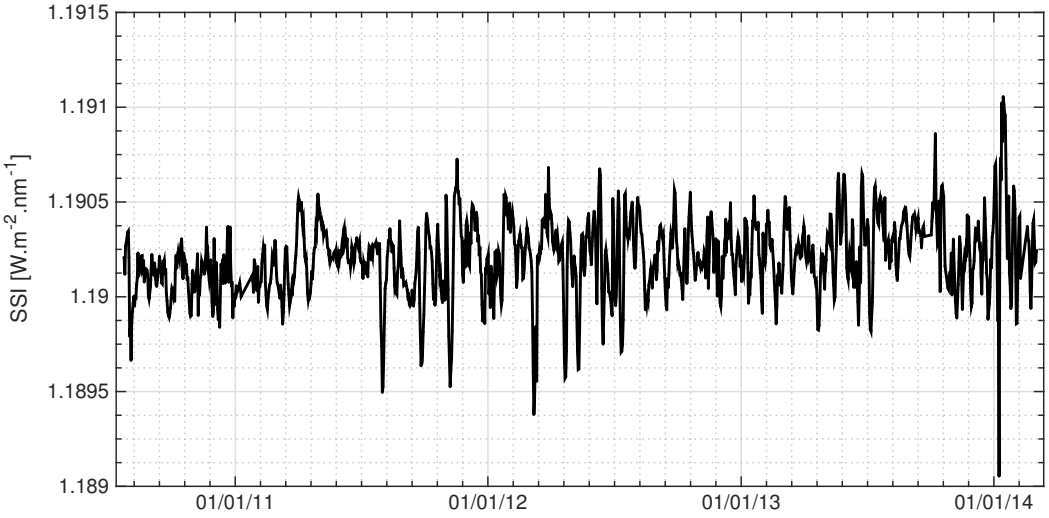

Figure 4: Evolution of the SSI as seen by the SES at 782 nm (in black).

Currently, we use SODISM Level 1 (L1) data taking into account dark signal and flat-field corrections. Several simple image-processing methods (edge detectors as Canny or Sobel, filtering, and segmentation process) have been tested in order to detect the sunspots and faculae on the SODISM solar images (L1 data) that allows SSI reconstruction. However, these methods did not provide robust and efficient results. For this purpose, a large amount of approaches have been developed and implemented. The review made by Zharkov et al.[14] evaluates and summarizes existing manual, semi-automated and fully automated feature recognition techniques applied to the different solar features including sunspots and faculae.

A fully automated recognition methods has been developed for sunspots and faculae detections, using morphological operators, partially combined with a region growing approach. Morphological tools have already been considered by Curto et al.[15] only for sunspots detection.

Figure 5 displays a detection on SODISM image (at 393.37 nm) after performing the 5 steps described below.

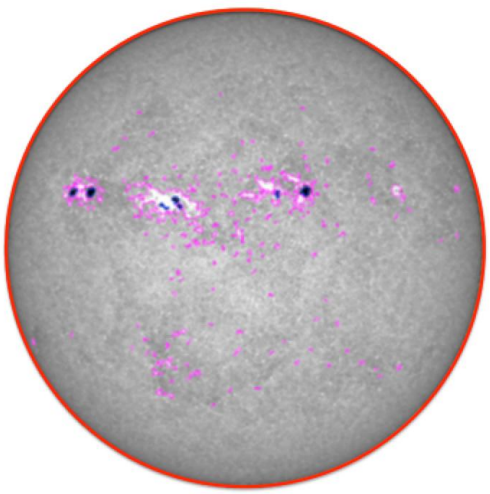

Figure 5: Example of solar disc segmentation that allows SODISM SSI reconstruction at 393.37 nm. The solar disc is represented by the red contour. The sunspots detection is shown in blue contour. The faculae detection is shown in magenta contour. The quality of the detection is governed by the thresholds used.

3.3.1 Preprocessing of SODISM Images

A preprocessing step is applied on the SODISM image (L1 data) in order to obtain a full contrasted image, and thus an automatic, easier and more accurate detection. First, a median filter is applied to reduce the noise over

the image. The resulting image is directly used to detect the solar disc contour and the sunspots. For faculae detection, this preprocessing step is not sufficient enough to obtain an accurate detection. More processing must be done on the input image for it to be contrasted enough to detect automatically faculae. Hence, a closing operation followed by an intensity rescale is applied. Then, for SODISM images, a blind deconvolution and an histogram equalization are also needed. The resulting image is then used for the faculae detection.

3.3.2 Solar Disc Contour

The solar disc is automatically detected on the preprocessed SODISM image. An opening transformation is performed on the preprocessed SODISM image, then, a threshold is used to detect the solar disc contour.

3.3.3 Automatic Thresholds for Sunspots and Faculae Detections

The automatic thresholds for sunspots and faculae detection depend on the image, its brightness, and its contrast. For SODISM images, only the solar disc area is taken into account for the threshold determination. The pixels outside of the solar disc are not appropriate. The threshold detection is done on the preprocessed images. On SODISM images, the Otsu threshold[16] is not so suitable. Another method based on the histogram of the interior solar disc pixels was used. Since the thresholds are computed on the preprocessed images and the preprocessing is different whether the objects to detect are sunspots and faculae, the thresholds found are different for both detections, even if the same method is used to compute them.

3.3.4 Sunspots Detection

The sunspots detection is done with the preprocessed input image, on which an additional image-optimizing step is applied in SODISM images. It consists in morphological operations (a top-hat operation followed by a bottom-hat operation). Finally, a contrast enhancement technique is applied. The resulting image can be used for the sunspot detection. If a manual threshold has been entered, it is used for the detection. Otherwise, the algorithm computes and applies the most accurate threshold to correctly detect the sunspots. The Otsu threshold[16] used on SODISM images is accurate enough for the sunspots detection.

3.3.5 Faculae Detection

The faculae detection is done on the preprocessed SODISM image. The automatic threshold is found on the complemented preprocessed SODISM image. Finding a suitable threshold for the faculae detection has proven more difficult than evaluating the threshold for the sunspot detection. So the estimated automatic threshold is tested and corrected as followed to make sure that it is the most accurate. The threshold found is applied to the image, in order to detect faculae. If the number of detected faculae is not coherent, an iterative procedure is launched, starting from a reduced threshold and/or increasing it gradually until the number of detected faculae belongs to a fixed interval. Then, a region growing is done on the input image in order to obtain a more contrasted image, with more visible faculae. These steps are the most time consuming.

For each facula detected, a small threshold is used (0.1) to start the region growing. The region is iteratively grown by comparing all unallocated neighboring pixels to the region. The difference between a pixel's intensity value and the region's mean is used as a measure of similarity. The pixel with the smallest difference measured this way is allocated to the region. This process stops when the intensity difference between region mean and the new pixel become larger than the entered threshold or if the number of detected pixels increases dramatically. If the region growing for faculae is successful, the threshold is increased by 0.01 and the region growing is launched again in order to find the biggest region possible. This step returns a black image with the white grown faculae. It is then added to the input image, to increase the faculae and thus, the faculae detection. Then, the faculae detection is launched again on this image. The threshold is computed again on the new input image, and the detection is done with this threshold, and without a new region growing step. This detection process is particularly applicable for SODISM images at 393.37 nm.

3.3.6 Conclusion

This work is still in progress. When all corrections will be made on SODISM images, this method will be applied to all the images.

4. SOLAR OBLATENESS

Solar oblateness is a fundamental parameter of the Sun, which provides indirect information on the inner rotation profile and on the distribution of matter. However, the measurement of the solar oblateness ($\Delta R/R_\odot$) is difficult. $R_\odot$ represents the solar radius at one astronomical unit. The PICARD measured solar equator-to-pole radius difference ($\Delta R = R_{eq} - R_{pol}$) is close to 8 milli-arc-second (mas) for measurements in the photosphere. Different methods were developed.[17,18] Main results are given in Table 1. We have developed another new method based on a correction of the solar radius for a given solar angle according to the brightness of the limb at the inflection point position and its derivative with solar radius. We found ΔR results that are close to those published previously ($\sim$8 mas). From this method, we find a solar equator-to-pole radius difference at 393.37 nm of 16.4$\pm$3.1 mas for measurements made between 2010 and 2011. This result is surprising and requires further study. Similarly, a theoretical study is needed to understand why the solar equator-to-pole radius difference in the chromosphere is higher than that obtained in the photosphere.

Table 1: PICARD solar equator-to-pole radius difference (ΔR).

Date	Authors	ΔR [mas]	Instrument (remark)
2010–2011	This work (new method)	16.4 $\pm$3.1 (1σ)	SODISM (λ=393.37 nm)
2011	Irbah et al. (2014)[17]	8.4 $\pm$0.3 (1σ)	SODISM (λ=535.7 nm)
2010–2011	Meftah et al. (2014)[18]	7.9 $\pm$0.3 (1σ)	SODISM (λ=782.2 nm)

5. PICARD HELIOSEISMIC STUDIES WITH SODISM

SODISM also allows us to conduct a program for helioseismology in intensity at 535.7 nm. Main results are given in Corbard et al. (2013).[19] In this section, we show main results about solar internal flows from SODISM.

With relative precisions below 10^{-5} obtained for thousand of measured oscillation frequencies, helioseismology is probably one of the most important field of solar metrology. The analysis of the helioseismic signal gives us the ability to infer internal flows (rotation and meridional circulation), which are a crucial part for any model aiming at reproducing the solar magnetic cycle. While internal rotation can be deduced from global helioseismology, meridional flows are inferred using local techniques (ring diagrams or time-distance), which were until recently limited to area relatively close to the surface. One of the most debated topic therefore concerns the detection of the return flow of meridional circulation.

As a reminder, the PICARD space mission (2010-2014) was mainly dedicated to measurement of the global parameters of the Sun. The SODISM instrument however also offers the possibility of inferring internal properties of the Sun through helioseismology *i.e.* by monitoring its oscillations revealed by its global and local scale intensity fluctuations. The helioseismology program of PICARD was described by Corbard et al. (2008).[20]

The Helioseismic and Magnetic Imager (HMI) onboard Solar Dynamics Observatory (SDO) is mainly dedicated to helioseismology from Doppler measurements but it also provides continuum intensity images that can be analyzed through the same pipeline as the one developed for SODISM. We first present the results obtained in terms of internal rotation from SODISM signal. We report an attempt to use time distance analysis on large area of low resolution images and comparative measurements between velocity and intensity observables in order to infer travel times originating from the deep meridional flow down to the solar tachocline.

5.1 Internal Rotation Rate

Figure 6 shows the regularized least square (RLS) inversion of the measured rotational splittings of 769 modes from l =1 to l =99. For a given mode (n,l), each m-spectrum were individually fitted. An expansion on orthogonal polynomials with up to 9 coefficients was then determined on the m-frequencies which passed some quality criteria. The steep gradient of the tachocline at the base of the convection zone is clearly seen in our data. The inferred rotation rate in the convection zone is similar to the one usually obtained from velocity data.

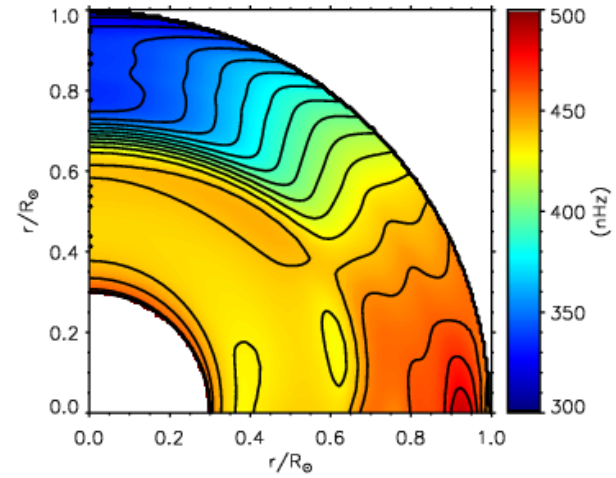

Figure 6: Internal Solar rotation rate inferred by inverting frequency splittings from SODISM intensity images over the period from April 16 to November 10, 2011. The solution is not reliable bellow 0.63 solar radius and is poorly constrained close to the pole. Only the symmetric part with respect to the equator can be obtained. The inverse method used is a 2D regularized least square.

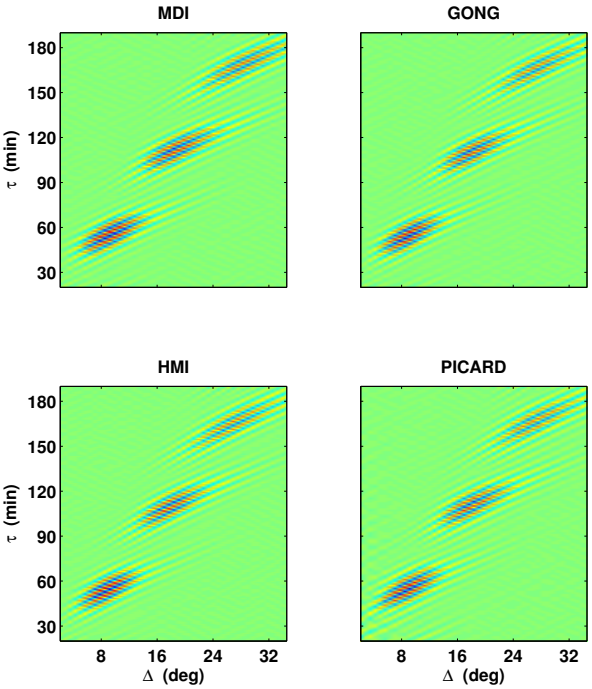

Figure 7: Multi-bounce cross-correlation functions of 4 different datasets (from the Michelson Doppler Imager (MDI) instrument onboard SoHO, from GONG, from HMI, and from PICARD/SODISM) show good agreement.

5.2 Deep Meridional Circulation Signature

In an attempt to infer the deep meridional flow down to the tachocline using the intensity data of SODISM, we have followed the technique developed for the Global Oscillation Group (GONG) data.[21,22] Analysis steps are described below:

- We first selected 374 days of SODISM 'Macro Pixel' images by visually inspecting the daily l-ν diagrams. These selected days present very few temporal aliasing and relatively low spatial noise.
- Each image is then remapped with tracking (within $\pm 60^o$ of latitudes and taking into account the differential rotation), each day being tracked separately (reference time is noon).
- A 30 minutes running mean is subtracted.
- A spherical harmonics (SH) decomposition (for l=0 to 300) of each daily set is performed and time series of SH coefficients are obtained.

- Phase-velocity filters, standard in time-distance analysis, are then applied to SH time series.
- Images are reconstructed back in latitude-longitude domain using the filtered SH coefficients.
- Cross correlation functions (CCF) are then computed for the different angular distances (Figure 7) and phase and group times were obtained by Gabor fitting the CCFs (Figure 8).
- Finally, meridional flow time differences (Northware-Southware travel times) are estimated (Figure 9).

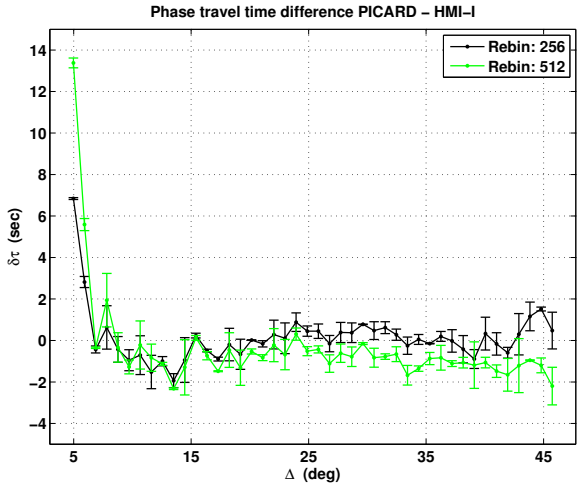

Figure 8: Differences between phase travel times measured from SODISM and HMI intensity images. The two curves show two different rebining of HMI images. We obtain large differences for small angular distances and we see some influence of the rebining at large angular distances (*i.e.* for deeper flow).

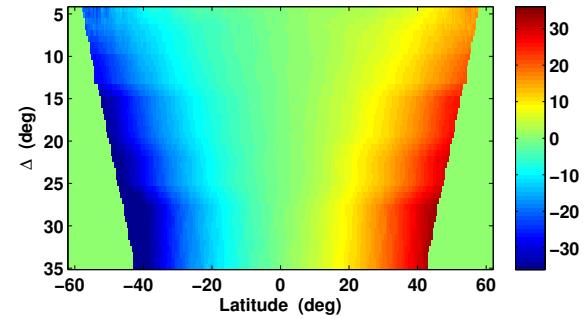

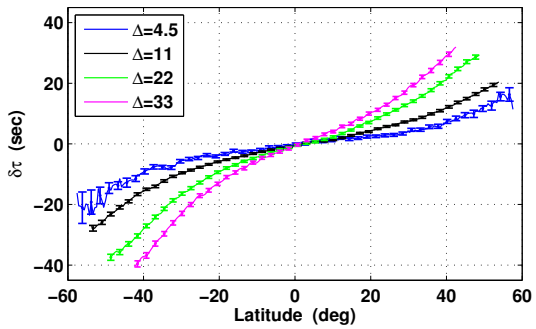

Figure 9: (top) Time-differences map as a function of distance and latitude. By increasing the distance we loose the second point in high latitudes, so the highest latitude reached decreases with increasing distance.
(bottom) Four horizontal cuts of the time- differences map. Lower turning points for these distances are approximately: 0.973, 0.933, 0.865 and 0.79 solar radius.

5.3 Results and Discussions

The calibration procedure of SODISM images is quite complicated and we have to face strong instrumental and orbital effects that affect both the photometric signal and the geometry of the solar images. There are still ongoing efforts to re-calibrate these images (correction for ghost images, charge-coupled device (CCD) persistence,

flat-fielding *etc.*). However, we have demonstrated that the current version of the dataset has permitted to infer solar internal flows using the techniques of helioseismology.

In a first step, we have shown that we were able to measure the frequency splittings of global modes accurately enough in order to infer the internal rotation rate down to the tachocline from the SODISM intensity signal. The internal rotation rate profile obtained (Figure 6) is in good agreement with the one deduced from simultaneous HMI data.

In a second step, our goal is to use SODISM images in order to get the signature the deep meridional flow which is a much more difficult task for any helioseismic instrument. This measurement is notably known for being affected by systematic center-to-limb variation.[23] The inter-comparison of different instruments is therefore crucial and the specificities of SODISM images (intensity signal) may be of particular interest.

One first result is that, the magnitude of the travel time differences measured from SODISM intensity images is much higher than the typical travel times obtained from Doppler images. Velocities show typically 1-2 seconds time differences while intensity signal shows up to 30 seconds. This is consistent with the results of Zhao et al. (2012).[23]

From the analysis of the north-south travel time differences, we have obtained a first signature of a deep meridional flow increasing with depth (Figure 9). It has however been shown by Zhao et al. (2012)[23] that this signal should be corrected from measurements made in the East-West direction. Our attempts to make such correction using SODISM images were so far not successful, we are still working on that aspect.

6. SOLAR RADIUS

6.1 Absolute Determination

Solar radius determination is one of the oldest problems in Astronomy, which is one of the age-old natural sciences. In fact, the measurement of the sizes of the different bodies in the solar system and the distances between them has been a primary challenge. Thus, systematic measurements of the solar radius have been made since Antiquity. First determinations of solar radius with visual method were obtained by Aristarchus (270 B.C.), Archimedes (230 B.C.), and Al-Battani (880). The most common solar radius definition is based on the determination of the inflection point position (IPP) of the solar limb darkening function (LDF). The PICARD mission contributes to the absolute solar radius determination quest. PICARD provides the value of the solar radius at different wavelengths. The SODISM solar radius results (photospheric continuum), using the method described by Meftah et al. (2014)[4] are listed in Table 2. The SODISM II solar radius results (photospheric continuum and "chromospheric") are listed in Table 2. PICARD Ca II K filters have a wide bandwidth ($\Delta\lambda$) of 0.7 nm over the core at 393.37 nm, which covers all the K1, K2, and K3 regions. Thus, PICARD Ca II K imagery reveals magnetic structures of the Sun from about 450 to 2000 km above the photosphere. Through PICARD observations, we can determine the absolute value of the photospheric and specific "chromospheric" solar radius.

Table 2: Summary of the PICARD solar radius observations at different wavelengths. S represents the standard deviation of the mean value (σ=1). A represents the absolute uncertainty (σ=1) in the determination of the solar radius with random and systematic errors. $\Delta\lambda$ corresponds to the bandwidth of the central wavelength (λ) of the filter. [(a)] The solar radius is based on the determination of the inflection point position.

λ [nm]	$\Delta\lambda$ [nm]	Radius at 1 AU [(a)]	S (arc-seconds)	A (arc-seconds)	Experiment	References
535.7	0.5	959.83 arc-seconds	±0.15	±0.36	SODISM	This work
607.1	0.7	959.86 arc-seconds	±0.06	±0.20	SODISM	[4]
782.2	1.6	959.91 arc-seconds	±0.19	±0.34	SODISM	This work
393.37	0.7	961.360 arc-seconds	±0.106	±0.387	SODISM II	This work
535.7	0.5	959.777 arc-seconds	±0.125	±0.194	SODISM II	[5]
607.1	0.7	959.862 arc-seconds	±0.126	±0.185	SODISM II	[5]
782.2	1.6	959.876 arc-seconds	±0.099	±0.129	SODISM II	[5]
1025.0	6.4	959.832 arc-seconds	±0.181	±0.105	SODISM II	[5]

6.2 Solar Radius Variations

The measurements of the solar radius variations are difficult to make but very important. They provide additional informations on the behaviour of the Sun, which can help to better understand the internal solar structure that still has a lot of uncertain aspects. The investigation of the solar radius variability can greatly help to discern between different class of solar models available up today. Indeed, a solar model contains our best knowledge of the physical phenomena, which we think, are governing the Sun's functioning. To validate a model, its predictions are compared with all available observations (intensity of the magnetic fields, TSI, SSI, distribution of the active regions, *etc.*). Any new physical amount thus makes possible to improve our understanding of the solar physics phenomena.

The constant or variable solar radius is a contribution to elucidate the origin of the solar activity, phenomenon related to the magnetic fields of surface or below within the convective zone. Thus, the variation of the solar radius or its constancy must be established without ambiguity. PICARD provides solar radius variation during Solar Cycle 24.

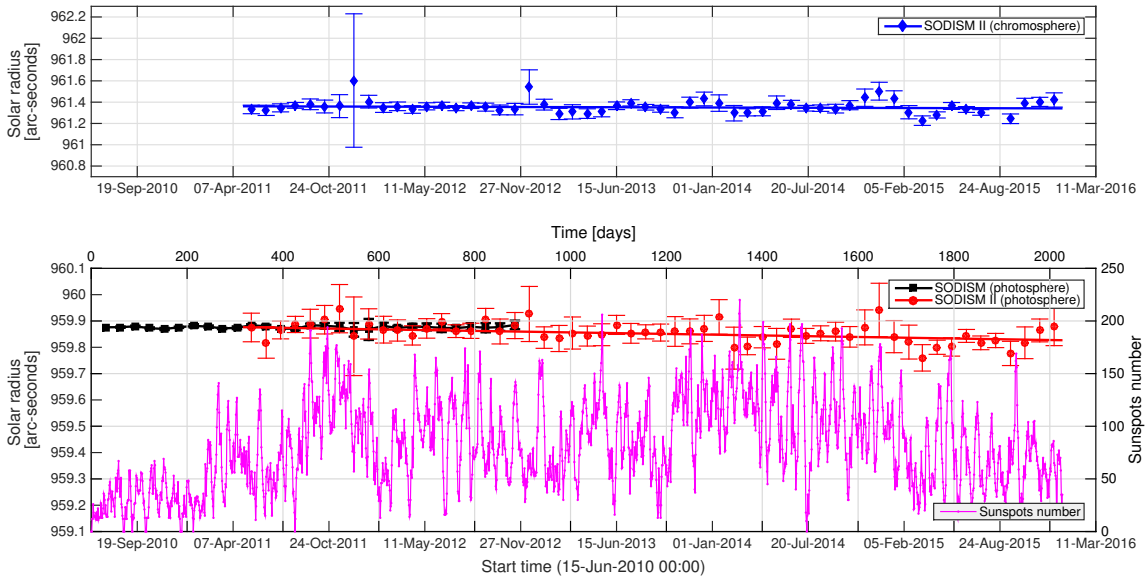

Figure 10: PICARD monthly mean solar radius evolution (photosphere and chromosphere) *vs.* sunspots number. In orbit ($\sim$ 730 km altitude), SODISM performed corrected measurements of the solar radius between August 2010 and December 2012 (at 782.2 nm). On the ground (at Calern, France), the SODISM II telescope has been carrying out complementary measurements since May 2011 (at 393.37 nm & 782.2 nm).

From 2010 to 2014, the solar radius has been measured by the SODISM space-based telescope on board PICARD, which has suffered substantial degradation due to harsh space environment. Consequently, as with MDI, the SODISM raw measurements require a thermo-optical correction. Thus, the evolution of the SODISM solar radius at one astronomical unit is given in the Figure 10 (at 782.2 nm). Changes in the solar radius are smaller than 20 milli-arc-second (mas) peak-to-peak (monthly mean).[24] But even more interesting, SODISM corrected measurements highlight a solar periodicity of 129.5 days with 13 mas variation peak-to-peak (sinusoidal fit with daily mean data between mid-2010 and January 2012 where the SODISM correction is effective). In order to further look for periodicities, we computed the Lomb-Scargle periodograms using the corresponding time-series as given above, and with estimates of significance levels against the null hypothesis of random noise. In that case, the $\sim$130-days period is found significant at the 99% confidence level (4.6 mas root mean square (rms)).

The PICARD ground-based instrument (SODISM II) represents a tool to generate the needed long-term time-series of the solar radius. Indeed, PICARD measurements show the benefit of simultaneous measurements obtained from ground and space observatories as a joint venture. As a result, these two means are complementary from each other. In fact, the solar radius observed with SODISM II (393.37 nm and 782.2 nm) since May 2011

results from small variations after 60 months of measurements (Figure 10). The SODISM II solar radius at one astronomical unit decreases at a rate of ∼-10±6 mas per year (2σ) for the photospheric channel (at 782.2 nm). At 393.37 nm (chromosphere), the linear trend is close to zero (with a significant uncertainty). Thus, the photospheric non-significant trend could be from solar, and/or atmospheric, and/or instrumental origin such as the significance of the chromospheric trend.

On can notice than SODISM II ground measurements provides solar radius variations, which are higher than SODISM space measurements (Table 3 and Figure 11), mainly due to the effects of the atmosphere. This work is under investigation (high cooperation between LATMOS and OCA teams).

Table 3: Solar radius periodicities with statistical significance level of over 99% (results obtained from Lomb-Scargle periodograms). Long periodicities (greater than 300 days) are not resolved due to PICARD short periods of observation.

Instrument	Period [days]	Variations [mas rms]
SODISM	129.5	4.6
(Jul. 2010–Jan. 2012)	–	–
SODISM II	18.4	14.5
(May 2011–May 2015)	24.3	16.2
	31.8	14.2
	35.6	12.0
	36.7	12.5
	65.1	11.5
	74.0	14.8
	79.5	14.9
	99.3	11.8
	108.4	11.1
	119.4	13.5
	131.4	13.4
	146.0	12.9

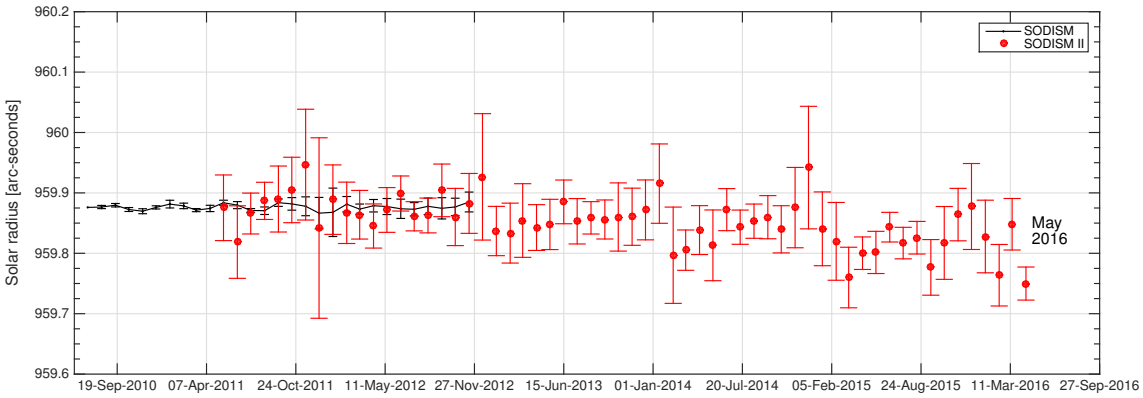

Figure 11: PICARD solar radius variations after six years of observations (photosphere).

7. CONCLUSIONS

PICARD gives new estimates of the absolute values of the total solar irradiance. Both radiometers of the PICARD mission provide TSI values close to 1361–1362 Wm^{-2}.

SSI measurements from 2010 to 2014 in different spectral bands (at 210, 215, 266, 535, 607, and 782 nm) were obtained with PICARD space instruments (PREMOS and the SES). An effort is underway (image-processing methods) to provide other SSI variations over time with the SODISM telescope (particularly at 393.37 nm). From the full corrections on SODISM images, we hope to get new SSI results. Indeed, SODISM has a sufficient quality to feed SSI models.

From the PICARD mission, the solar equator-to-pole radius difference was determined at different wavelengths after correcting measurements for optical distortion and for SODISM instrument temperature trend. PICARD mission provides solar equator-to-pole radius difference close to 8 milli-arc-seconds in the photosphere. We have not observed any correlation between equator-to-pole radius difference (or oblateness) and solar activity. In the chromosphere, the solar equator-to-pole radius difference as seen by SODISM is close to 16 milli-arc-seconds. This result is surprising and still under investigation.

PICARD has a program of helioseismology in intensity at 535.7 nm. In this paper, we provide results about solar internal flows from SODISM. Another work is under evaluation with SODISM. It concerns three consecutive days dedicated to helioseismic measurements at 393.37 nm without interruption. We have obtained a l-ν diagram computed from these observations (limb images at 393.37 nm), which requires a comparison with that obtained at 535.7 nm. As a reminder, the l-ν diagram shows how much acoustic energy there is at each frequency for every one of the spatial modes of solar oscillations.

PICARD gives new estimates of the absolute values of the solar radius in different spectral bands (535.7, 607.1, and 782.2 nm). In the photosphere, the PICARD solar radius are close to 959.9 arc-seconds, which are slightly higher than the canonical value of Auwers (959.63 arc-seconds). At 393.37 nm (Ca II K with $\Delta\lambda$=0.7 nm), the PICARD solar radius is close to 961.4 arc-seconds, which covers all the K1, K2, and K3 region. From 2010 to 2014, the solar radius has been measured by the SODISM space-based telescope on board PICARD, which has suffered substantial degradation due to harsh space environment. From a thermo-optical correction, changes in the solar radius are smaller than 20 milli-arc-second. Moreover, the solar radius observed with SODISM II (393.37 nm and 782.2 nm) since May 2011 results from small variations after 60 months of measurements. The SODISM II solar radius at one astronomical unit decreases at a rate of $\sim$-10$\pm$6 mas per year (2σ) for the photospheric channel (at 782.2 nm). At 393.37 nm (chromosphere), the linear trend is close to zero (with a significant uncertainty). Thus, the photospheric non-significant trend could be from solar, and/or atmospheric, and/or instrumental origin such as the significance of the chromospheric trend.

The above results ensue from a sustained effort to calibrate and exploit scientifically PICARD observations in their current state. These are now publicly available online at the MEDOC center: `http://idoc-picard.ias.u-psud.fr/sitools/client-user/Picard/project-index.html`. The scientific program is still ongoing and future versions of the data products are to be expected within months. The reader is thus invited to keep up his/her interest for the mission and for its subsequent updates.

ACKNOWLEDGMENTS

PICARD is a mission supported by the French space agency (CNES), CNRS, the Belgian Space Policy (BELSPO), the Swiss Space Office (SSO), and the European Space Agency (ESA). We thank CNRS, LATMOS, OCA, IAS, CNES, RMIB, PMOD, ROB, and the French Alternative Energies and Atomic Energy Commission (CEA).

REFERENCES

1. Schmutz, W., Fehlmann, A., Hülsen, G., Meindl, P., Winkler, R., Thuillier, G., Blattner, P., Buisson, F., Egorova, T., Finsterle, W., Fox, N., Gröbner, J., Hochedez, J.-F., Koller, S., Meftah, M., Meisonnier, M., Nyeki, S., Pfiffner, D., Roth, H., Rozanov, E., Spescha, M., Wehrli, C., Werner, L., and Wyss, J. U., "The PREMOS/PICARD instrument calibration," *Metrologia* **46**, S202–S206 (Aug. 2009).
2. Conscience, C., Meftah, M., Chevalier, A., Dewitte, S., and Crommelynck, D., "The space instrument SOVAP of the PICARD mission," in [*SPIE*], *Society of Photo-Optical Instrumentation Engineers Conference Series* **8146** (Sept. 2011).
3. Meftah, M., Dewitte, S., Irbah, A., Chevalier, A., Conscience, C., Crommelynck, D., Janssen, E., and Mekaoui, S., "SOVAP/ Picard, a Spaceborne Radiometer to Measure the Total Solar Irradiance," *Solar Phys.* **289**, 1885–1899 (May 2014).

4. Meftah, M., Hochedez, J.-F., Irbah, A., Hauchecorne, A., Boumier, P., Corbard, T., Turck-Chièze, S., Abbaki, S., Assus, P., Bertran, E., Bourget, P., Buisson, F., Chaigneau, M., Damé, L., Djafer, D., Dufour, C., Etcheto, P., Ferrero, P., Hersé, M., Marcovici, J.-P., Meissonnier, M., Morand, F., Poiet, G., Prado, J.-Y., Renaud, C., Rouanet, N., Rouzé, M., Salabert, D., and Vieau, A.-J., "Picard SODISM, a Space Telescope to Study the Sun from the Middle Ultraviolet to the Near Infrared," *Solar Phys.* **289**, 1043–1076 (Mar. 2014).
5. Meftah, M., Corbard, T., Irbah, A., Ikhlef, R., Morand, F., Renaud, C., Hauchecorne, A., Assus, P., Borgnino, J., Chauvineau, B., Crepel, M., Dalaudier, F., Damé, L., Djafer, D., Fodil, M., Lesueur, P., Poiet, G., Rouzé, M., Sarkissian, A., Ziad, A., and Laclare, F., "Ground-based measurements of the solar diameter during the rising phase of solar cycle 24," *Astron. Astrophys.* **569**, A60 (Sept. 2014).
6. Ikhlef, R., Corbard, T., Morand, F., Renaud, C., Fodil, M., Ziad, A., Borgnino, J., Meftah, M., Assus, P., Chauvineau, B., Hauchecorne, A., Lesueur, P., Poiet, G., Ubaldi, F., Hamadouche, M., and Abdelatif, T., "MISOLFA: a generalized monitor for daytime spatio-temporal turbulence characterization," *Mon. Not. Roy. Astron. Soc.* **458**, 517–530 (May 2016).
7. Kopp, G. and Lean, J. L., "A new, lower value of total solar irradiance: Evidence and climate significance," *Geophys. Res. Lett.* **38**, 1706 (Jan. 2011).
8. Fröhlich, C., Romero, J., Roth, H., Wehrli, C., Andersen, B. N., Appourchaux, T., Domingo, V., Telljohann, U., Berthomieu, G., Delache, P., Provost, J., Toutain, T., Crommelynck, D. A., Chevalier, A., Fichot, A., Däppen, W., Gough, D., Hoeksema, T., Jiménez, A., Gómez, M. F., Herreros, J. M., Cortés, T. R., Jones, A. R., Pap, J. M., and Willson, R. C., "VIRGO: Experiment for Helioseismology and Solar Irradiance Monitoring," *Solar Phys.* **162**, 101–128 (Dec. 1995).
9. Schmutz, W., Fehlmann, A., Finsterle, W., Kopp, G., and Thuillier, G., "Total solar irradiance measurements with PREMOS/PICARD," in [*American Institute of Physics Conference Series*], *American Institute of Physics Conference Series* **1531**, 624–627 (May 2013).
10. Fehlmann, A., Kopp, G., Schmutz, W., Winkler, R., Finsterle, W., and Fox, N., "Fourth World Radiometric Reference to SI radiometric scale comparison and implications for on-orbit measurements of the total solar irradiance," *Metrologia* **49**, S34–S38 (Apr. 2012).
11. Cessateur, G., Schmutz, W., Wehrli, C., Gröbner, J., Haberreiter, M., Kretzschmar, M., Rozanov, E., Schöll, M., Shapiro, A., Thuillier, G., Egorova, T., Finsterle, W., Fox, N., Hochedez, J.-F., Koller, S., Meftah, M., Meindl, P., Nyeki, S., Pfiffner, D., Roth, H., Rouzé, M., Spescha, M., Tagirov, R., Werner, L., and Wyss, J.-U., "Solar irradiance observations with PREMOS filter radiometers on the PICARD mission: In-flight performance and data release," *Astron. Astrophys.* **588**, A126 (Apr. 2016).
12. Harder, J., Lawrence, G., Fontenla, J., Rottman, G., and Woods, T., "The Spectral Irradiance Monitor: Scientific Requirements, Instrument Design, and Operation Modes," *Solar Phys.* **230**, 141 (Aug. 2005).
13. Meftah, M., Hauchecorne, A., Irbah, A., Cessateur, G., Bekki, S., Damé, L., Bolsée, D., and Pereira, N., "Solar Spectral Irradiance at 782 nm as Measured by the SES Sensor Onboard Picard," *Solar Phys.* (Apr. 2016).
14. Zharkov, S., Zharkova, V., Ipson, S., and Benkhalil, A., "Technique for Automated Recognition of Sunspots on Full-Disk Solar Images," *EURASIP Journal on Applied Signal Processing* **2005**, 318462 (Dec. 2005).
15. Curto, J. J., Blanca, M., and Martínez, E., "Automatic Sunspots Detection on Full-Disk Solar Images using Mathematical Morphology," *Solar Phys.* **250**, 411–429 (Aug. 2008).
16. Otsu, N., "A Threshold Selection Method from Gray-level Histograms," *IEEE Transactions on Systems, Man and Cybernetics* **9**, 62–66 (Jan. 1979).
17. Irbah, A., Meftah, M., Hauchecorne, A., Djafer, D., Corbard, T., Bocquier, M., and Momar Cisse, E., "New Space Value of the Solar Oblateness Obtained with PICARD," *Astrophys. J.* **785**, 89 (Apr. 2014).
18. Meftah, M., Irbah, A., Hauchecorne, A., Corbard, T., Turck-Chièze, S., Hochedez, J.-F., Boumier, P., Chevalier, A., Dewitte, S., Mekaoui, S., and Salabert, D., "On the Determination and Constancy of the Solar Oblateness," *Solar Phys.* **290**, 673–687 (Mar. 2015).
19. Corbard, T., Salabert, D., Boumier, P., Appourchaux, T., Hauchecorne, A., Journoud, P., Nunge, A., Gelly, B., Hochedez, J. F., Irbah, A., Meftah, M., Renaud, C., and Turck-Chièze, S., "Helioseismology with PICARD," *Journal of Physics Conference Series* **440**, 012025 (June 2013).
20. Corbard, T., Boumier, P., Appourchaux, T., Jiménez-Reyes, S. J., Gelly, B., and PICARD Team, "Helioseismology program for the PICARD satellite," *Astronomische Nachrichten* **329**, 508–516 (June 2008).
21. Kholikov, S., Serebryanskiy, A., and Jackiewicz, J., "Meridional Flow in the Solar Convection Zone. I. Measurements from GONG Data," *Astrophys. J.* **784**, 145 (Apr. 2014).
22. Kholikov, S. and Hill, F., "Meridional-Flow Measurements from Global Oscillation Network Group Data," *Solar Phys.* **289**, 1077–1084 (Apr. 2014).
23. Zhao, J., Nagashima, K., Bogart, R. S., Kosovichev, A. G., and Duvall, Jr., T. L., "Systematic Center-to-limb Variation in Measured Helioseismic Travel Times and its Effect on Inferences of Solar Interior Meridional Flows," *Astrophys. J. Lett.* **749**, L5 (Apr. 2012).
24. Meftah, M., Hauchecorne, A., Irbah, A., Corbard, T., Ikhlef, R., Morand, F., Renaud, C., Riguet, F., and Pradal, F., "On the Constancy of the Diameter of the Sun during the Rising Phase of Solar Cycle 24," *Astrophys. J.* **808**, 4 (July 2015).